Hindawi
Advances in Meteorology
Volume 2022, Article ID 9181219, 18 pages
https://doi.org/10.1155/2022/9181219

Research Article

Geometric and Physical Characteristics of Precipitation Clouds in Tibetan Plateau

Kunyu Teng,[1] **Hongke Cai**,[2] **Xiubin Sun**,[1] **and Quanliang Chen**[2]

[1]*College of Electronic Engineering, Chengdu University of Information Technology, Chengdu 610225, China*
[2]*School of Atmospheric Science, Chengdu University of Information Technology/Plateau Atmosphere and Environment Key Laboratory of Sichuan Province, Chengdu 610225, China*

Correspondence should be addressed to Quanliang Chen; chenql@cuit.edu.cn

Received 13 September 2021; Revised 4 December 2021; Accepted 21 December 2021; Published 10 January 2022

Academic Editor: Hiroyuki Hashiguchi

This paper examines the basic geometric and physical characteristics of precipitation clouds over the Tibetan Plateau, based on the Tropical Rainfall Measuring Mission (TRMM) Precipitation Radar (PR) data from 1998 to 2015, using the minimum bounding rectangle (MBR) method. The results show that about 60% of the precipitation clouds occur with a scale of approximately 18 km (length) and 15 km (width), and the proportion of precipitation clouds with a length longer than 100 km and a width wider than 90 km is less than 1%. Most of the precipitation cloud exhibits a shape between square and long strips in the horizontal direction and lanky in the vertical direction. The average rainfall intensity of precipitation clouds is between 0.5 and 6 mm h^{-1}. The average length and width of precipitation clouds show a logarithmic, linear relationship. The distribution of raindrops in precipitation clouds is relatively compact. With the expansion of the area, the precipitation clouds gradually become squatty. The relationship between physical and geometric parameters of precipitation clouds shows that with the precipitation cloud area expanding, the average rainfall rate of precipitation clouds also increases. Heavy convective rainfall is more likely to occur in larger precipitation clouds. For the precipitation clouds of the same size, the area fraction and contribution of convective precipitation are lower than that of stratiform precipitation.

1. Introduction

Cloud is an important indicator of weather and climate changes. It plays an important role in the global energy and water cycle, which is called the "regulator" of radiation balance in the earth-atmosphere system. Clouds can change the local atmospheric energy balance and affect the atmospheric circulation and energy cycle by reflecting and absorbing solar short-wave radiation and absorbing and emitting Earth long-wave radiation [1–4]. During the formation of different types of clouds, the thermodynamic and microphysical processes are different, which can result in different radiative forcing and climate feedback [5, 6]. Among them, the study of precipitation clouds is particularly critical. At first, the precipitation clouds were usually considered as circular precipitation areas, and their rainfall rates (or radar reflectivity) were equal to or greater than the threshold rainfall rates (or radar reflectivity) [7]. Capsoni et al. [8] defined precipitation clouds as regions with rain rates (RR) greater than 5 mm h^{-1} observed by *S*-band radar near Milan during April–October 1980. In addition, the formulas of spatial numerical density and cumulative rainfall rate distribution of precipitation clouds are obtained. In 1989, Awaka [9] revised the formulas and set the threshold of rainfall rate at 0.4 mm h^{-1}. Studies about the characteristics of precipitation clouds is typically important for in-depth studies of the formation mechanism of precipitation, the simulation of the impact on future climate changes, the weather forecast, and the water resources forecast. Moreover, understanding the structure of precipitation clouds is also of great significance to carry out operations of influencing weather in scientific and artificial approaches.

For a long time, many scholars have been studying the climatic characteristics of clouds in China and its surrounding areas by using ground observation data and various satellite observation data. The results pointed out that the annual average total cloud coverage in southern China is more than that in northern China. And the east and west sides of the Tibetan Plateau have high annual average total cloud coverage. The distribution characteristics of low clouds are consistent with the total cloud coverage, and the distribution of cloud optical thickness and water vapor content is also similar to that of total cloud coverage. In all types of clouds in China and its surrounding areas, except cumulus, stratocumulus, and rain layer clouds, the cloud thickness of southern China is greater than that of northern China. The largest average thickness among all types of clouds is the deep convective cloud, and the smallest one is the stratocumulus. The occurrence probability of cloudy sky in southern mainland China is higher than in northern mainland China, and the occurrence probability of single-layer clouds is significantly higher than that of multilayer clouds. The occurrence probability of clouds of summer and autumn is higher than that of spring and winter. In summer, the cloud height has the maximum value for each layer of clouds [10–12]. Cirrus clouds are the most common in Northwest China. The optical thickness and cloud water path can have maximum value for the following clouds: water layer cloud, ice layer cloud, water rain layer cloud, ice rain layer cloud, and the deep convective cloud. The high-value areas of cloud coverage are located in the areas of Tianshan-Kunlun-Qilian Mountains and southern Shanxi province, which are beneficial to artificial water enhancement [10, 13]. In southern China's summer time, the frequency of stratospheric precipitation is more than twice as much as that of convective precipitation, and the intensity of convective precipitation is at least 4 times as much as that of stratospheric precipitation, and convective precipitation mainly occurs in the afternoon [14].

The Tibetan Plateau, known as the "roof of the world", is the largest plateau in China and the highest in the world. It is the birthplace of many rivers in China, with high-mountain rivers, steep and changeable terrain, and complex topography. The Tibetan Plateau is in the middle and upper troposphere, and its atmospheric activity is intense and frequent, which has a significant impact on climate change locally and globally. Due to the complex topography and the thermodynamic structure, the weather and the climate phenomena of the Tibetan Plateau and their corresponding mechanisms have been attracting a number of scholars. Two large-scale scientific experiments were carried out in China in 1979 and 1998 (the third is 2014–2021, which is still ongoing), and remarkable results have been achieved. The relevant studies on the Tibetan Plateau show that the Tibetan Plateau is dominated by convective clouds in summer, which is mainly distributed in the central and eastern parts of the plateau and southeastern Tibet [15]. The precipitation on the Tibetan Plateau is mainly concentrated in southeastern Tibet, and the maximum near-surface precipitation rate is greater than 100 mm h^{-1} [16]. The water vapor content in the UTLS (upper troposphere to lower stratosphere) region of the southern Qinghai-Xizang Plateau is higher than that of the northern Qinghai-Xizang Plateau [17, 18]. The frequency of deep convection on the southern slope of the plateau is higher than that on the plateau. And the deep convection mainly occurs from July to August [19].

The average altitude of the Tibetan Plateau is more than 4000 m. Its complex topography and thermodynamic structure make the clouds on the plateau unique. Therefore, many scholars have done a lot of research on plateau clouds. The initial research can only be based on the ground observation data to study the basic parameters such as cloud coverage and height. The results show that the distribution of total cloud coverage in the plateau decreases from southeast to northwest, and there is a significant downward trend when we analyze it year by year or season by season. Strong convective clouds have the highest frequency in summer and the lowest frequency in winter [20, 21]. After the emergence of satellite data, the studies of plateau clouds are not limited to cloud coverage and cloud height. The results show that the clouds on the top of the Tibetan Plateau are higher than those of the surrounding area [22]. There are few clouds on the north and south sides of the plateau, and the optical thickness of the cloud is also small [23]. The optical thickness of the cloud is large in the areas with more clouds on the western and southeastern Tibetan Plateau [24]. The total cloud coverage in the eastern plateau is more than that in the central and western plateau, and the total cloud coverage of the southern Tibetan Plateau is more than that in the northern Tibetan Plateau. The total cloud coverage of the edge of the plateau is more than that of the main part of the plateau [25]. The distribution of total cloud coverage on the plateau shows a decreasing trend from southeast to the northwest of the plateau [26]. The optical thickness of clouds, cloud water path, and cloud top temperature on the plateau have all increased significantly [27].

Studies about the macro and microcharacteristics of precipitation clouds on the plateau play an important role in understanding the thermal-dynamic and microphysical processes, water vapor transportation, and climate changes in the formation of precipitation clouds on the plateau. Many scholars have used various satellite data to study precipitation clouds on the plateau. Fu et al. [28] studied the precipitation cloud structure in a valley and its nearby areas in the southeast of the Tibetan Plateau by using the TRMM satellite precipitation radar. The results show that topographic forcing is an important external factor for the formation of this precipitation cloud cluster. The maximum length of the precipitation cloud system is more than 100 km, and its width is about 40 km. It is a strong convective cloud cluster. Other research has shown that the summer precipitation on the plateau is dominated by deep and weak convective precipitation, followed by shallow and thin precipitation, and deep and strong convective precipitation is the least. In summer, the frequency and intensity of precipitation on the Tibetan Plateau gradually increase from west to east, while the heights of cloud tops and precipitation echo tops have exactly the opposite trend. The main precipitation on the plateau in summer is dominated by ice precipitation, and the plateau clouds are dominated by single-layer clouds [29, 30].

Summarizing the previous studies, it can be found that the research on the plateau precipitation cloud is mainly focused on the investigation of the summer season. And most of the research is related to the horizontal distribution, vertical structure, and microphysical characteristics, but there is still a lack of research on other aspects, such as the geometric characteristics of precipitation clouds, the relationship between geometric size and precipitation, and the contribution of different types of precipitation to the same precipitation clouds. Therefore, this paper is using TRMM/PR data from 1998 to 2015 to study the geometric and physical characteristics of precipitation clouds in the Tibetan Plateau.

2. Data and Methodology

2.1. Introduction. In this study, the standard dataset of TRMM 2A25 at version 7 from January 1998 to December 2015 (https://trmm.gsfc.nasa.gov/data_dir/data.html) was used. The Tropical Rainfall Measuring Mission (TRMM) is the first Earth Science mission dedicated to studying tropical and subtropical rainfall. The Japanese space agency (JAXA) launched the satellite on an H-II rocket from Tanegashima Space Center on November 27, 1997. It is a nonsun-synchronous, about 16 orbits every day, with an inclination of 35 degrees to the Equator, and a precession period of about 46 days for the orbit nodes with respect to the Sun. The main parameters of PR are as follows: scans across a swath 215 km (245 km after boost) wide, vertical and horizontal resolutions of 250 m and 4.3 km at nadir (5.0 km after boost), the detection height is from the surface up to a height of about 20 kilometers. According to TRMM's precipitation algorithm, the 2A25 precipitation profile data also provides precipitation type information, which is divided into convective precipitation, stratiform precipitation, and other types of precipitation. To put it simply, the identification of the precipitation type is based on whether the radar echo has a bright band and whether the echo intensity exceeds 39 dBZ. The bright band is a sign of identifying stratiform clouds, and 39 dBZ is the standard for identifying convective precipitation. Nonconvective and nonstratigraphic precipitation are defined as "other" types of precipitation. The scope and topography of the research area are shown in Figure 1.

2.2. Research Methods. Regarding the research methods of precipitation clouds, most scholars use the ellipse-fitting approach to filter precipitation clouds and to determine the orientation angle and the length of the major and minor axes of precipitation clouds. Comparative analysis of precipitation cloud systems in tropical and subtropical, ocean and land [31–33]. However, this method has some limitations in the identification of precipitation clouds and errors due to swath truncation effect.

In 2020, Fu et al. [34] used the minimum bounding rectangle (MBR) method to identify precipitation clouds and then obtained the shape parameters of precipitation clouds, which effectively avoided the swath truncation effect and was an effective screening for precipitation clouds method. It showed that MBR method is an effective method of identifying precipitation clouds. Therefore, this study uses the Minimum Bounding Rectangle (MBR) method to identify precipitation clouds. The precipitation pixel track truncation identification will be performed first, that is, whether the precipitation pixels are traversed close to the edge of the track. If there are precipitation pixels at the edge of the track, these precipitation clouds will be defined as truncated precipitation clouds and will be eliminated. The study of Hirose et al. showed that due to the radial distortion of TRMM PR scanning, the geometric distortion of edge pixels is more significant than that of the near nadir pixels, but the land deviation is smaller [35]. Moreover, we eliminate edge pixels, which reduce the impact of pixel distortion on the results, so our research is still very meaningful. Then, it is necessary to rotate the minimum bounding rectangle to fit the spatial distribution of target precipitation clouds to ensure accurate precipitation clouds are identified. The length (L) of the rain cell is the distance between the two ends of the target precipitation cloud along the direction with the longer edge of the smallest bounding rectangle. Similarly, the other direction along the smallest bounding rectangle is defined as the width (W) of the precipitation cloud. Both L and W are the horizontal dimensions of precipitation cloud. The MBR method is used to identify precipitation clouds, which can be relatively easily applied to search for tens of thousands of rain pixels in PR swath. At the same time, compared with the ellipse-fitting approach, the MBR method can improve the inclusion integrity of the rain pixels in the target precipitation cloud. To describe the three-dimensional geometric characteristics of precipitation clouds, this paper gives a series of parameters based on the study of Fu et al. [34], including length (L), width (W), height (H_{avgc} and H_{avgs}), area (S), and others. The geometric parameters are shown in Table 1.

In addition, the physical parameters of precipitation clouds are defined as well. Based on rain types, rain rate profiles and near-surface rain rate supplied at version 7 2A25, those physical parameters of the precipitation cloud are shown in Table 2. These parameters are important for expressing the intensity, inhomogeneity, and evolution stages of precipitation clouds.

For example, Figure 1 shows two precipitation clouds selected by the MBR method, namely June 15, 1998 and August 7, 1998. Table 3 shows the calculated geometric and physical parameters of the two precipitation clouds displayed in Figure 2.

The first case (Figure 2(a)) is a mesoscale precipitation cloud. Its length is 155.08 km, and its width is 134.6 km, and its area is 8438.75 km^2. The average echo top height is 10.1 km, and the maximum echo top height is 16.25 km. Since $\alpha = 0.87$, we can know that the precipitation cloud is a quasisquare precipitation cloud. In addition, since $\beta = 0.52$, we can see that the distribution of raindrops in the precipitation clouds is relatively compact. From the perspective of spatial morphology, the precipitation cloud has $\gamma_{\max} = 0.11$ and $\gamma_{\text{avg}} = 0.07$, indicating that its spatial morphology is "squatty," and the vertical scale is much smaller

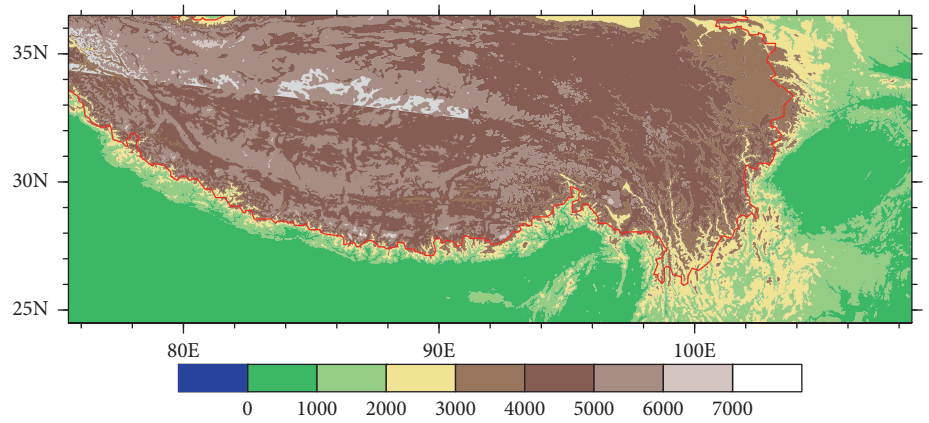

Figure 1: Topographic map of the Tibetan Plateau (The red line represents the 3000-meter contour).

Table 1: The definition of geometric parameters of precipitation clouds.

Symbol	Geometric meaning
L(km)	The length of precipitation cloud
W(km)	The width of precipitation cloud
α	α describing horizontal shape of precipitation cloud, $\alpha = W/L$
S(km^2)	The area of precipitation cloud, sum of all area of rain pixels
β	The filling ratio of precipitation cloud, the ratio of precipitation cloud S to the fitted MBR area
H_{max}(km)	The maximum echo top height among rain pixels in precipitation cloud
H_{avg}(km)	The mean echo top height averaged among rain pixels in precipitation cloud
γ_{max}	The maximum spatial morphology, γmax = Hmax/L
γ_{avg}	The mean spatial morphology, γavg = 2 $*$ Havg/($L + W$)

Table 2: The definition of physical parameters of precipitation clouds.

Symbol	Physical meaning
RR_{avg}(mm·h^{-1})	Mean rain rate obtained averaged by all rain rate within precipitation cloud
RR_{max}(mm·h^{-1})	The maximum rain rate among rain pixels of precipitation cloud
RR_{avgc}(mm·h^{-1})	Mean convective rain rate averaged by all convective rain rate within precipitation cloud
RR_{avgs}(mm·h^{-1})	Mean stratiform rain rate averaged by all stratiform rain rate within precipitation cloud
RR_{maxc}(mm·h^{-1})	The maximum rain rate among convective pixels of precipitation cloud
RR_{maxs}(mm·h^{-1})	The maximum rain rate among stratiform pixels of precipitation cloud
CAF(%)	Fraction of convective area to total precipitation area within precipitation cloud
SAF(%)	Fraction of stratiform area to total precipitation area within precipitation cloud
CPC(%)	Convective precipitation contribution to total precipitation within precipitation cloud
SPC(%)	Stratiform precipitation contribution to total precipitation within precipitation cloud

Table 3: The calculated (horizontal and vertical) and physical parameters of the first/second case.

Geometrical parameters		Physical parameters	
L (km)	155.08/188.44	RR_{avg}(mm·h^{-1})	2.57/1.95
W (km)	134.60/63.33	RR_{max}(mm·h^{-1})	124.85/69.88
A	0.87/0.34	RR_{avgc}(mm·h^{-1})	10.00/7.76
S (km^2)	8438.75/4199.75	RR_{avgs}(mm·h^{-1})	1.59/1.41
β	0.52/0.45	RR_{maxc}(mm·h^{-1})	124.85/69.88
H_{max} (km)	16.25/8.5	RR_{maxs}(mm·h^{-1})	11.54/5.00
H_{avg} (km)	10.10/5.92	CAF(%)	11.86/8.5
γ_{max}	0.11/0.045	SAF(%)	86.51/91.5
γ_{avg}	0.07/0.047	CPC(%)	46.19/33.91
		SPC(%)	53.46/66.09

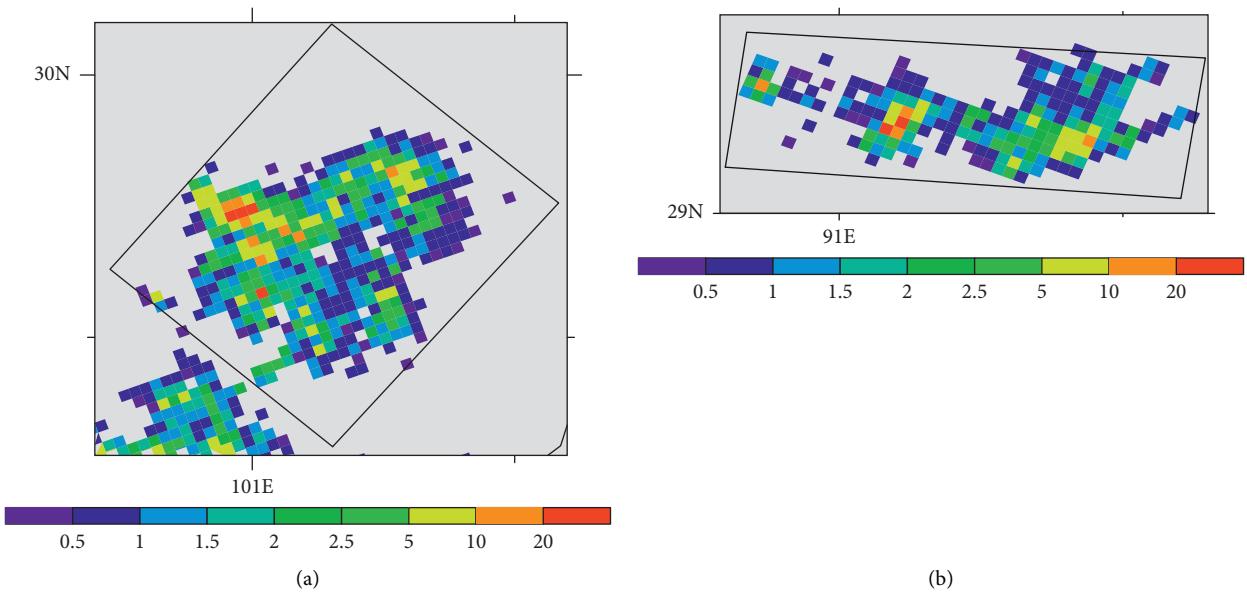

Figure 2: Near-surface rain rate of two precipitation clouds occurred on Tibetan Plateau ((a) 15 June 1998; (b) 7 August 1998) measured by PR.

than that in the horizontal direction. CAF = 11.86%, SAF = 86.51%, indicating that the stratiform precipitation in this precipitation clouds occupies a large area fraction. However, CPC = 46.19% and SPC = 53.46% indicate that although the area occupied by convective precipitation is smaller, the contribution of convective precipitation is greater. In this case, $RR_{avg} = 2.57$ mm h^{-1}, $RR_{max} = 124.85$ mm h^{-1}, $RR_{avgc} = 10$ mm h^{-1}, $RR_{avgs} = 1.59$ mm h^{-1}, $RR_{maxc} = 124.85$ mm h^{-1}, $RR_{maxs} = 11.54$ mm h^{-1}.

For the second case (Figure 2(b)), the precipitation cloud has a length of 188.44 km, width of 63.33 km, and area of 4199.75 km^2. The average echo top height is 5.92 km, and the maximum echo top height is 8.5 km. Different from the first case, its $\alpha = 0.34$ shows that the precipitation cloud is long strip shape. Its $\beta = 0.45$ shows that the distribution of raindrops in the precipitation cloud is not as compact as the first case. From the perspective of spatial morphology, the precipitation cloud has $\gamma_{max} = 0.045$ and $\gamma_{avg} = 0.047$, which shows that its spatial morphology is also "squatty," but its vertical scale is smaller than the first case. In addition, the CAF = 8.5% and SAF = 91.5% of this precipitation cloud indicate that the area fraction of stratiform precipitation in this precipitation cloud is larger than that of the first case. CPC = 33.91% and SPC = 66.09% indicate that although the contribution of convective precipitation is larger than that of the occupied area, the contribution of stratiform precipitation is still greater. In this precipitation cloud, $RR_{avg} = 1.95$ mm h^{-1}, $RR_{max} = 69.88$ mm h^{-1}, $RR_{avgc} = 7.76$ mm h^{-1}, $RR_{avgs} = 1.41$ mm h^{-1}, $RR_{maxc} = 69.88$ mm h^{-1}, $RR_{maxs} = 5$ mm h^{-1}.

We can conclude from the above two examples that the geometric and physical parameters of the two different types of precipitation clouds are different, and these parameters are well described by the MBR method. In this study, a total of 300,320 precipitation clouds were identified in the Tibetan Plateau from January 1998 to March 2015. The geometric and physical characteristics of these precipitation clouds will be discussed below.

3. Results and Discussion

3.1. Statistical Characteristics of Geometric and Physical Parameters. First, we show the statistical characteristics of precipitation clouds. The result indicates that the probability distribution functions (PDFs) of L reaches the peak of 60% when L is at 18 km, that is, the occurrence frequency of precipitation clouds with 18 km in length is 60% (Figure 3(a)). When L is greater than 18 km, the occurrence probability of precipitation clouds decreases with the increase of L. When L is greater than 100 km, the occurrence probability of precipitation clouds drops rapidly to below 1%. Similarly, the PDF of W reaches the peak of 60% when W is 15 km (Figure 3(b)). When W is greater than 90 km, the occurrence probability of precipitation clouds is very low, less than 1%. From the PDF of L and W, more than 60% of precipitation clouds appear on the scale of 18 km in length and 15 km in width. The statistics in Table 4 show that the average length of precipitation clouds in the Tibetan Plateau is 34.74 km and the average width is 19.91 km.

In terms of the level of precipitation clouds, the occurrence probability of precipitation clouds decreases with the increase of precipitation clouds area S (Figure 3(c)). When S is greater than 1000 km^2, the occurrence probability of precipitation clouds is less than 1%. The statistics in Table 4 show that the average area of precipitation clouds is 373.67 km^2.

The probability distribution function of the parameter α describing the horizontal shape of the precipitation cloud is shown in Figure 3(d). The results show that the occurrence probability of "long strip" ($\alpha < 0.4$) and "square" ($\alpha > 0.8$)

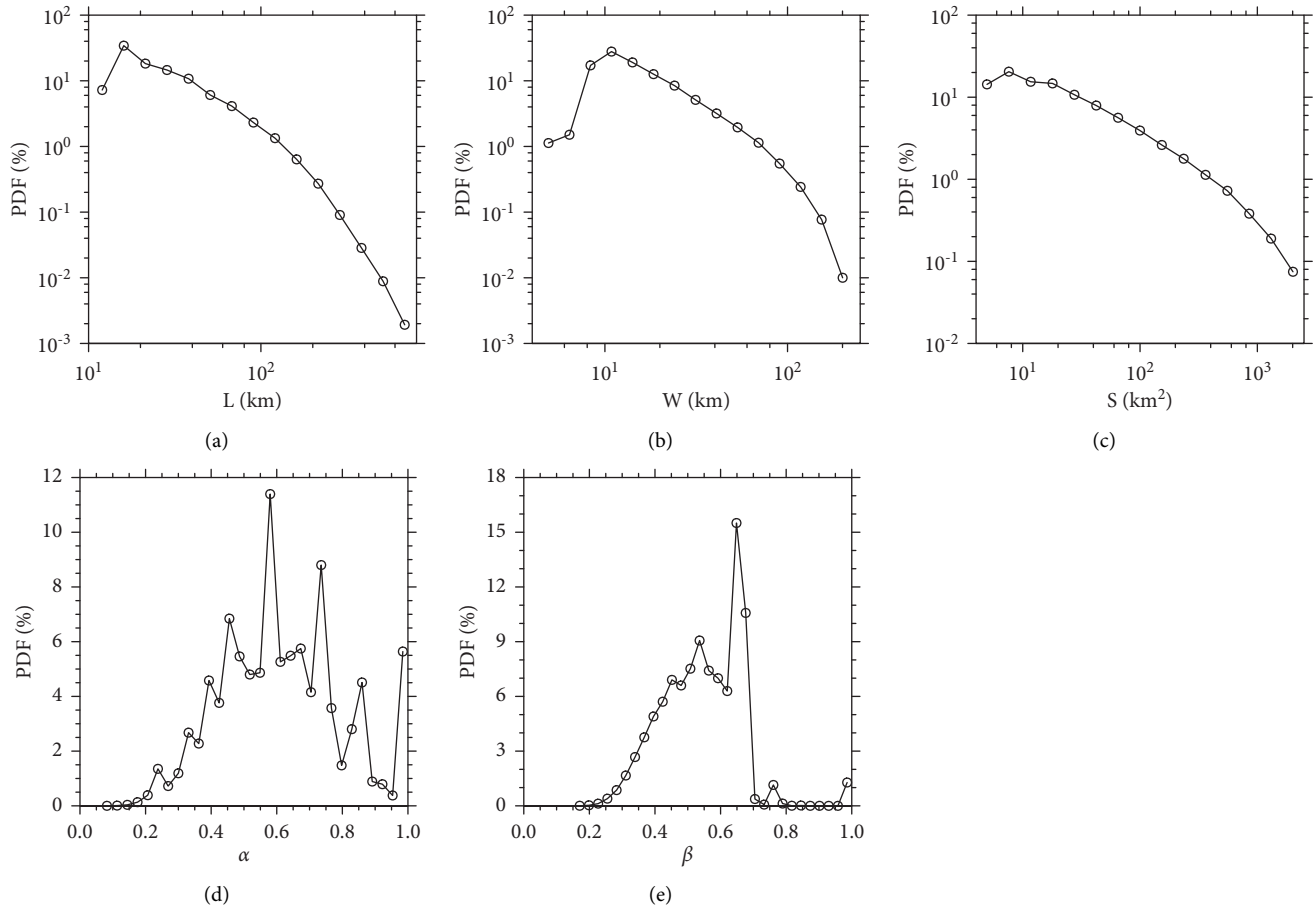

Figure 3: The probability distribution functions (PDFs) of the horizontal geometrical parameters for L (a), W (b), S (c), α (d), and β (e) on Tibetan Plateau calculated from 1998 to 2015.

Table 4: The calculated mean geometrical (horizontal and vertical) and physical parameters of precipitation clouds.

Geometrical parameters	Average	Physical parameters	Average
L (km)	34.74	RR_{avg}(mm·h^{-1})	1.54
W (km)	19.91	RR_{max}(mm·h^{-1})	5.60
α	0.62	RR_{avgc}(mm·h^{-1})	7.22
S (km^2)	373.67	RR_{avgs}(mm·h^{-1})	1.20
β	0.55	RR_{maxc}(mm·h^{-1})	13.61
H_{max} (km)	9.69	RR_{maxs}(mm·h^{-1})	2.60
H_{avg} (km)	8.36	CAF(%)	19.29
γ_{max}	0.39	SAF(%)	94.13
γ_{avg}	0.42	CPC(%)	44.16
		SPC(%)	86.39

precipitation clouds is relatively low, less than 15%. The rest precipitation clouds are featured between the two shapes. As shown in Table 4, the average α of precipitation clouds is 0.62. It can be seen that the average horizontal shape of most precipitation clouds is between square and long strips.

The PDF of β mainly varies between 0.25 and 0.75, with a peak value close to 0.7 (Figure 3(e)), and more than half of the precipitation clouds have β greater than 0.5. In fact, the average β of precipitation clouds in Table 4 is 0.55. These precipitation clouds almost fill more than half of the minimum bounding rectangle (MBR), which shows that the MBR method in this study is effective for identifying precipitation clouds.

The PDFs of vertical geometrical parameters of precipitation clouds over Tibetan Plateau calculated from 1998 to 2015 are plotted in Figure 4. The results show that the PDF of H_{max} has a peak at 9 km above the plateau (Figure 4(a)), with a range of 4–18 km. The average H_{max} of precipitation clouds is 9.69 km (Table 4). From the PDF of H_{avg} (Figure 4(b)), it can be seen that the H_{avg} value varies from 3 km to 13 km, and the peak appears at 9 km above the

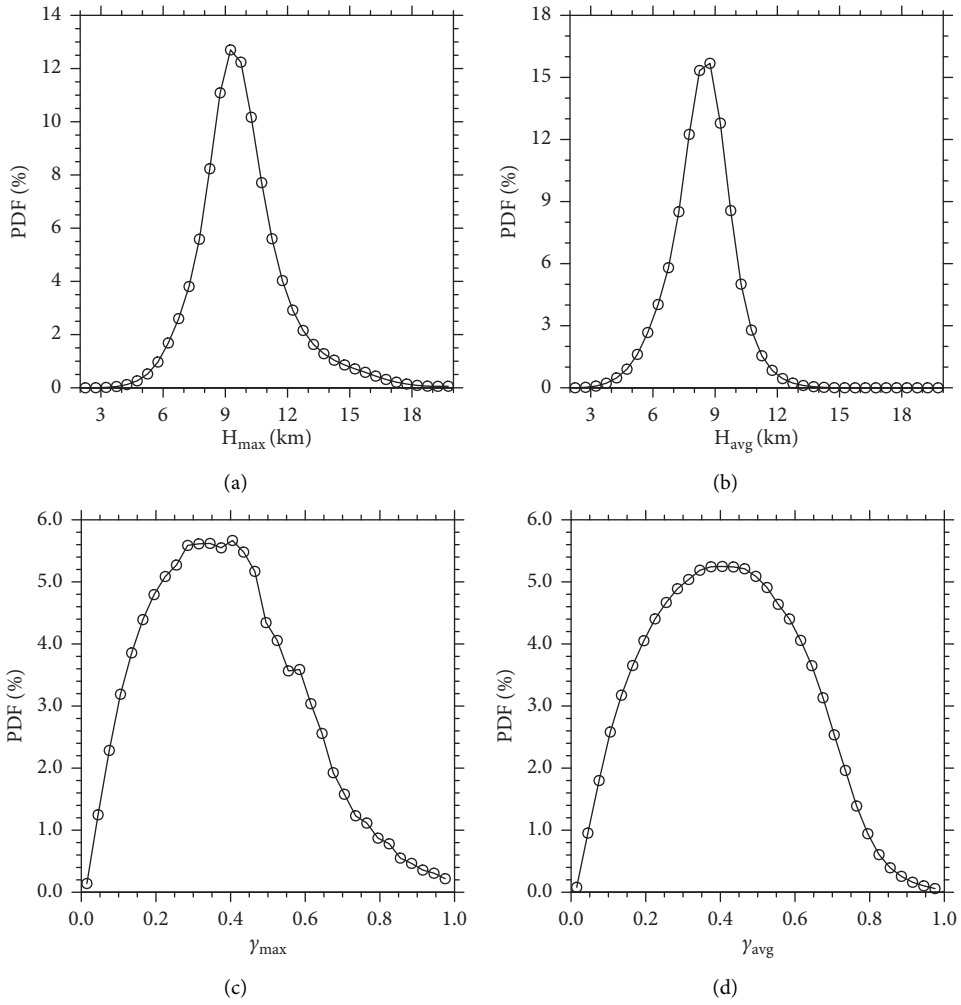

FIGURE 4: The PDFs of vertical geometrical parameters for H_{max} (a), H_{avg} (b), γ_{max} (c), and γ_{avg} (d) on Tibetan Plateau calculated from 1998 to 2015.

plateau. The statistical calculations in Table 4 show that the average H_{avg} of precipitation clouds is 8.36 km.

γ_{max} and γ_{avg} are parameters that reflect the spatial morphology of precipitation clouds, that is, the "squatty" appearance or "lanky" appearance of precipitation clouds. The variation range of γ_{max} and γ_{avg} is in 0.05–0.95, and both reach the peak value at 0.4 (Figures 4(c) and 4(d)). The mean γ_{max} and γ_{avg} are 0.39 and 0.42. It can be seen that the spatial morphology of precipitation clouds in the Tibetan Plateau is still dominated by "lanky" appearance.

Figure 5 shows the PDFs of these physical parameters of precipitation clouds in the Tibetan Plateau. The results show that the RR_{max} of precipitation cloud varies from 0.5 to 20 mm h^{-1}, with a peak at 1.5 mm h^{-1} (Figure 5(a)). The RR_{avg} of precipitation cloud varies from 0.5 to 6 mm h^{-1}, with a peak at 1 mm h^{-1} (Figure 5(b)). It can be seen from Figure 4(b) that the probability of heavy rain (RR_{avg} greater than 4 mm h^{-1}) on the plateau is much smaller than that of light rain (RR_{avg} less than 1.5 mm h^{-1}), and about 75% of precipitation clouds have RR_{avg} between 1.5 mm h^{-1} and 4 mm h^{-1}.

Figures 5(c)–5(f) show the PDFs of RR_{maxc}, RR_{avgc}, RR_{maxs} and RR_{avgs}. It can be seen that the difference between convective and stratiform precipitation is very obvious, and the variation range of convective precipitation is obviously larger than that of stratiform precipitation. The variation range of RR_{maxc} is 0.5–40 mm h^{-1}, the variation range of RR_{avgc} is 0.5–20 mm h^{-1}, and the variation range of RR_{maxs} and RR_{avgs} is only 0.5–9 mm h^{-1} and 0.5–3.5 mm h^{-1}. Both the RR_{maxc} and RR_{avgc} peaked at 6.5 mmh^{-1}, while the RR_{maxs} and RR_{avgs} peaks were at 2mmh^{-1} and 1mmh^{-1}, respectively. In Table 4, the statistical results show that the average precipitation cloud of RR_{maxc}, RR_{avgc}, RR_{maxs} and RR_{avgs} are 13.61 mm h^{-1}, 7.22 mm h^{-1}, 2.60 mm h^{-1} and 1.20 mm h^{-1}, respectively.

Through CAF or SAF, the area fraction of convective precipitation and stratiform precipitation, it also reflects the nature of precipitation clouds to a certain extent. For example, the raindrops in precipitation clouds are mostly convective or stratified. In Table 4, the average CAF and SAF of precipitation clouds is 19.29% and 94.13%. Figures 5(g) and 5(i) show the PDFs of CAF and SAF. The results show that the PDF decreases sharply with the increase of the CAF in the precipitation cloud, while the PDF increases sharply with the increase of the SAF in the precipitation cloud. The

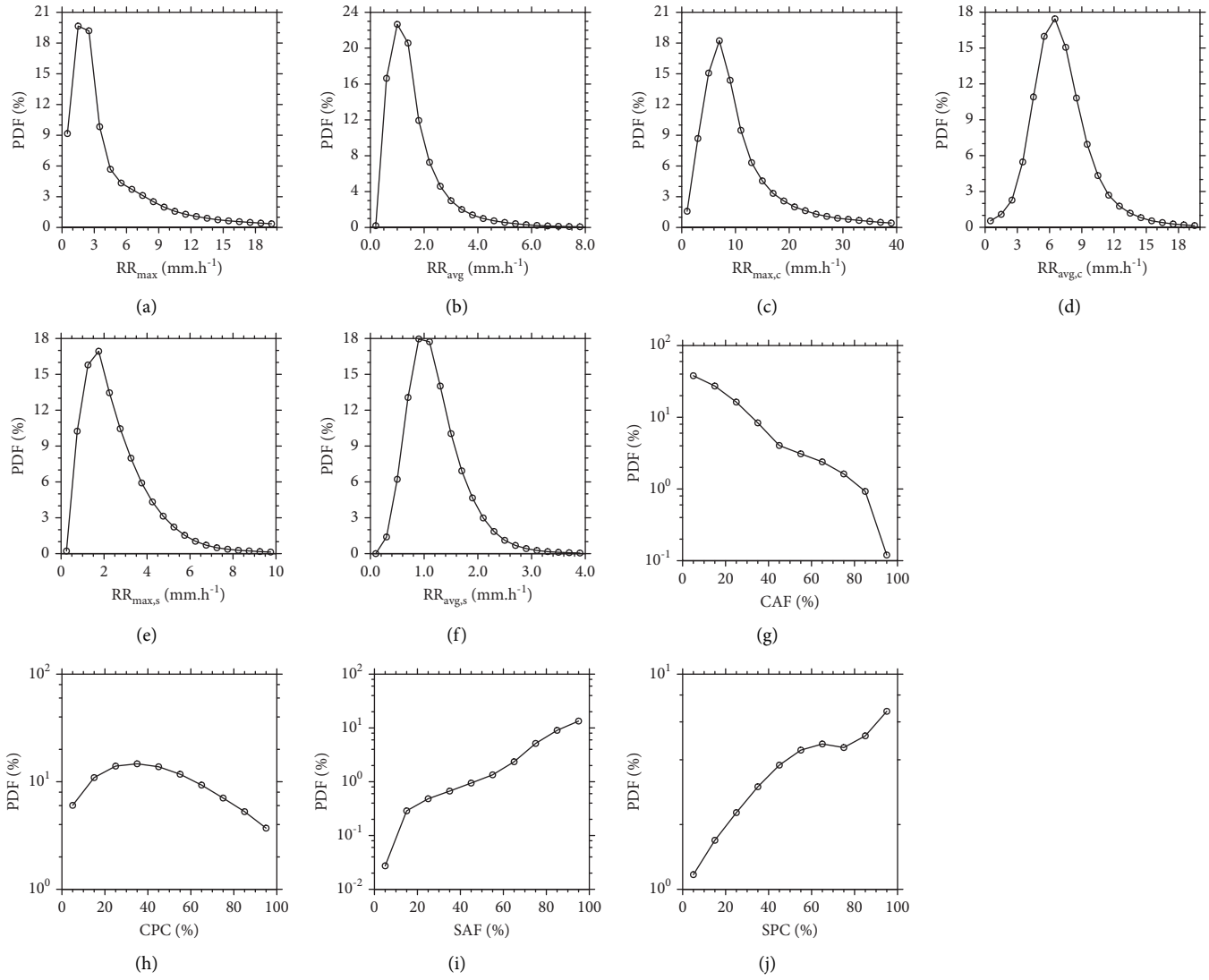

Figure 5: The PDFs of physical parameters for RR_{max} (a), RR_{avg} (b), RR_{maxc} (c), RR_{avgc} (d), RR_{maxs} (e), RR_{avgs} (f), CAF (g), CPC (h), SAF (i), and SPC (j) on Tibetan Plateau from 1998 to 2015.

CAF in 50% of the precipitation clouds on the plateau is less than 10%, but for the precipitation clouds with 80% CAF, it is only 1% on the plateau. On the contrary, the precipitation cloud with 40% SAF on the plateau is only 1%, but the precipitation cloud with 80% SAF has about 30%.

Figures 5(h) and 5(j) are the PDFs of CPC and SPC. The results show that when CPC increases to 20%, the PDF of CPC rises to more than 10%, and then as CPC increases to 100%, the PDF of CPC drops to below 10%. It can be seen that the contribution of convective precipitation in the same precipitation cloud is relatively low. When the SPC increases to 65%, the PDF of SPC rises from 1% to 7%. When the SPC increases to 75%, the PDF of SPC drops slightly. When the SPC increases to 100%, the PDF of SPC rises to the highest but still less than 10%. It can be seen that the contribution of stratiform precipitation in the same precipitation cloud is lower than that of convective precipitation.

The analysis of the above PDF shows that the MBR method can accurately identify precipitation clouds, and most precipitation clouds are 18 km in length and 15 km in width. The precipitation cloud with a length of more than 100 km, a width of more than 90 km, and an area of more than 1,000 km^2 is less than 1%. In contrast, the horizontal form of most precipitation clouds is long strip shape. From the vertical direction, the height of precipitation clouds is mostly 9 km above the plateau, and the spatial shape is mainly lanky appearance. The PDF of physical parameters indicates that the occurrence probability of light rain on the plateau is greater than heavy rain. The difference between convective and stratiform precipitation is very obvious. The area fraction of stratiform precipitation is greater than convective precipitation, but the contribution of precipitation is smaller than that of convective precipitation.

3.2. The Relationship among the Geometric Parameters. In this study, a total of about 300,000 samples of precipitation cloud geometric parameters were obtained. To increase the

reliability of statistical results, the approach of equal sample statistics is adopted. This approach has been used to calculate the mean and standard deviation of rain rate variation with altitude [36]. Specifically in this study, an independent variable (x axis) is divided into 40 intervals, 2.5% of the total samples in each interval, and then the values of a dependent variable (y axis) are averaged within each interval.

First, the relationship between L (x axis) and W (y axis) is shown in logarithmic coordinates in Figure 6. The results show that when L is greater than 25 km, L and W have a log-linear relationship, which can be expressed by the equation $\log W = a + b \times \log L$. Here, $a = 0.0798$ and $b = 0.8264$. When L is less than 25 km (W is less than 17 km), that is, a small precipitation cloud, the relationship between these two parameters is more complicated. For these precipitation clouds, these two parameters are geometrically affected by various combinations of raindrop positions, which may indicate that the horizontal geometric parameters at the initial stage of precipitation cloud formation have undergone strong physical changes.

In order to better understand the horizontal structure of precipitation clouds, the relationship between horizontal morphological parameters (α, β) and horizontal geometric parameters (L, W, S) is analyzed. As shown in Figure 7(a), as L increases from 10 km to 25 km, the parameter α decreases rapidly from 1.0 (square precipitation cloud) to 0.6 (quasisquare precipitation cloud). When L continues to increase from 25 km to around 300 km, α slowly decreases from 0.6 to around 0.5 (relatively long precipitation clouds). This confirms the characteristic of the ratio change between L and W shown in Figure 6; they generally follow a log-linear relationship. As shown in Figure 7(b), when W is greater than 17 km, the parameter α changes less. When W is less than 17 km, α increases with the increase of W, and α increases from 0.3 (long precipitation cloud) to 0.6 (quasisquare precipitation cloud).

The change in the ratio of L to W also determines that when S is less than 300 km^2, the parameter α (W/L) decreases with the increase of the precipitation cloud area S, which means that when the precipitation cloud area increases to 300 km^2, the shape of the precipitation cloud is very easy to change from a square shape to a relatively long strip shape. When S is greater than 300 km^2, α is almost unchanged. The above results show that the parameter α combined with the length and width of the precipitation area is also a parameter describing the horizontal shape of the precipitation cloud.

The parameter β is the ratio of the area of S to MBR. As shown in Figures 7(d)–7(f), when L is greater than 25 km, W is greater than 17 km, or S is greater than 300 km^2, β decreases with the increase of L, W and S, respectively. This means that the precipitation clouds on the plateau become loose when their horizontal geometric parameters are increased. For those precipitation clouds with small horizontal geometric parameters (L is less than 25 km, W is less than 17 km, or S is less than 300 km^2), the β of these precipitation clouds changes around 0.6 or above, indicating that the distribution of raindrops in these precipitation clouds is relatively compact.

Figure 8 shows the relationship between the vertical geometric parameters (H_{max} and H_{avg}) and the horizontal geometric parameters (L, W, and S) of precipitation clouds in the Tibetan Plateau. The results show that when L is less than 30 km, W is less than 18 km, and S is less than 200 km^2, there is no law for the change of H_{max} and H_{avg}, that is, the relationship between vertical geometric parameters and horizontal geometric parameters is more complicated. When L is greater than 30 km, W is greater than 18 km, and S is greater than 200 km^2, both H_{max} and H_{avg} tend to be stable, H_{max} is about 10 km and H_{avg} is about 8 km. Although the changing trends of H_{max} and H_{avg} are roughly the same, H_{avg} can more effectively express the relationship between the precipitation cloud range and the horizontal scale because it reduces the error caused by random values or extreme values.

The relationship between spatial morphology (γ_{max} and γ_{avg}) and S (Figure 9) shows that when S is less than 200 km^2, both parameters are greater than 0.3, which means that small precipitation clouds on the plateau tend to be a lanky appearance. Both parameters decrease with the increase of S, which indicates that as the area increases, the precipitation cloud gradually becomes a squatty appearance. This phenomenon is physically reasonable, because as the horizontal area of the precipitation cloud becomes larger, there is not enough energy to support its overall vertical development.

3.3. The Relationship between Physical and Geometric Parameters. The physical properties of precipitation clouds generally determine its geometric properties. Naturally, they are more concerned about the relationship between the physical parameters and geometric parameters of precipitation clouds. The relationship between RR_{max} (RR_{avg}) and S of precipitation clouds is shown in Figure 10. Relatively speaking, as S increases, the RR_{max} in the precipitation cloud increases (Figure 10(a)). It illustrates that in the larger precipitation cloud, the probability of extreme precipitation is greater. Compared with the relationship between RR_{max} and S, the relationship between RR_{avg} and S can more effectively understand the influence of precipitation cloud area on precipitation intensity. Because RR_{avg} is a parameter that normalizes all raindrops in a precipitation cloud, it reduces the influence of the unequal number of raindrops in different precipitation clouds. Figure 10(b) shows that, relatively speaking, as S increases, the precipitation cloud RR_{avg} increases. When S is greater than 500 km^2, RR_{avg} seems to remain at 1.7 mm h^{-1}.

The relationship between the precipitation cloud area S and the average rain rate and maximum rain rate of convective or stratiform precipitation, RR_{maxc}, RR_{maxs}, RR_{avgc} and RR_{avgs}, is obtained as plotted in Figure 11. Relatively speaking, RR_{maxc} and RR_{maxs} both increase with the increase of S. Both RR_{avgc} and RR_{avgs} also increase with the increase of S, but the increase of RR_{avgs} is not obvious. However, the growth rates of RR_{maxc} and RR_{maxs} exceed RR_{avgc} and RR_{avgs}, respectively.

Figure 12 shows the relationship between CAF (SAF) and S in the precipitation cloud and the relationship between

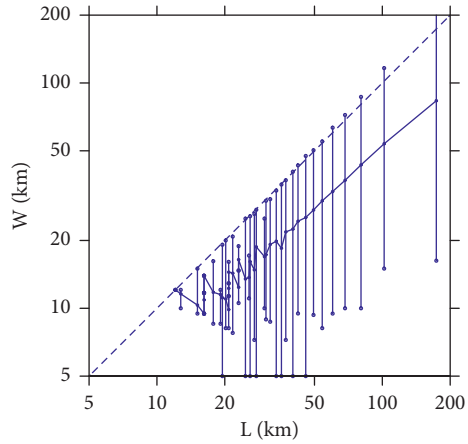

Figure 6: The relationship between W and L on Tibetan Plateau from 1998 to 2015 based on the statistical principle of same samples in each interval at x axis.

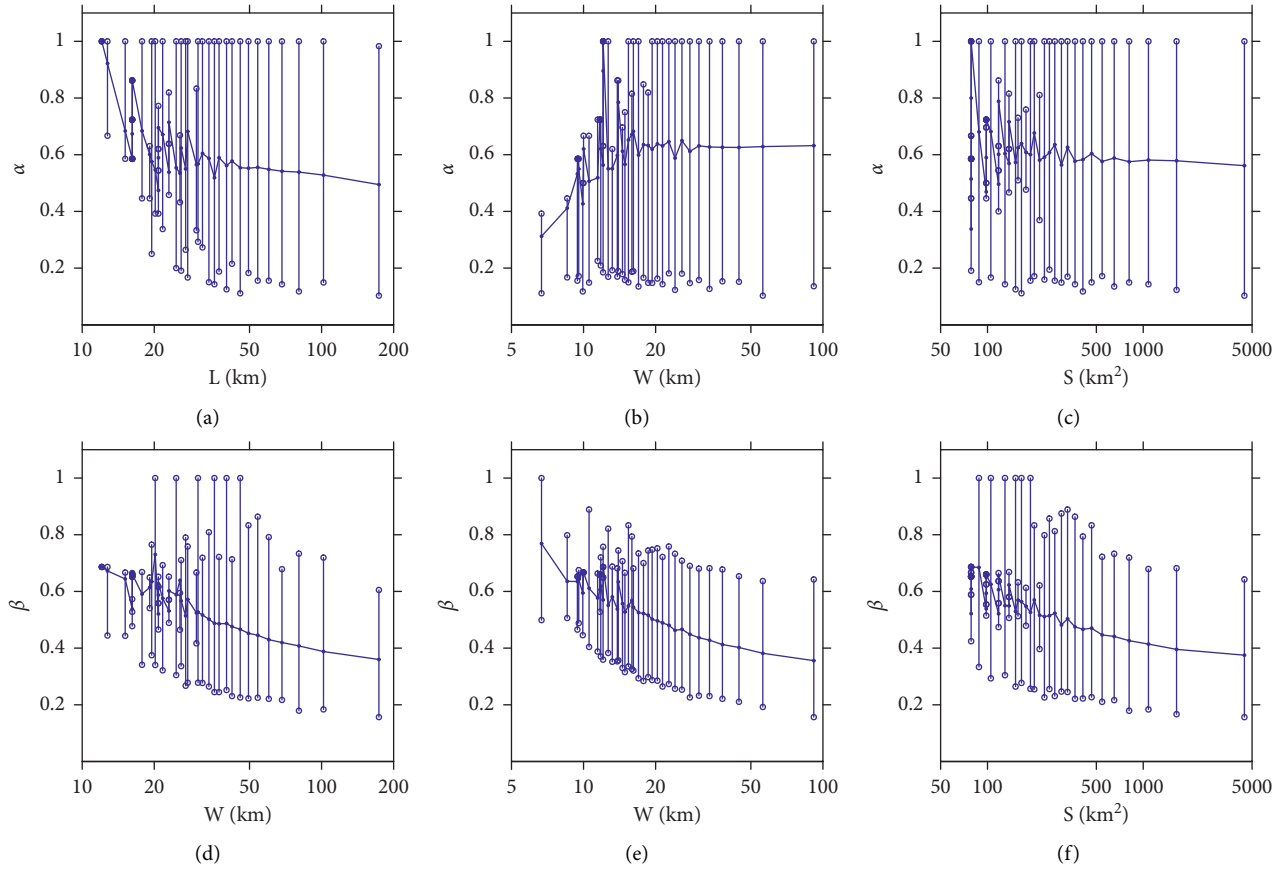

Figure 7: The relationship between α and L (a), α and W (b), α and S (c), β and L (d), β and W (e), and β and S (f) on Tibetan Plateau from 1998 to 2015 based on the statistical principle of same samples in each interval at x axis.

CPC (SPC) and S in the precipitation cloud. When S is less than 400 km^2, CAF is relatively high, which may be the initial development period of precipitation clouds. Then CAF gradually decreases to about 20%, which means that the precipitation cloud has entered a period of dissipation. In contrast, the relationship between SAF and S is significantly different from CAF. Figure 12(b) shows that as S increases from 50 to 5000 square kilometers, the value of SAF is almost all above 80%, indicating that the area fraction of stratiform precipitation is greater than convective precipitation and as much as 4 times larger. From Figures 12(c) and 12(d), it can be seen that the trend of CPC and SPC is roughly the same as CAF and SAF. When S is less than 400 km^2, CPC is relatively high, and then gradually decreases to about 40%. When S is

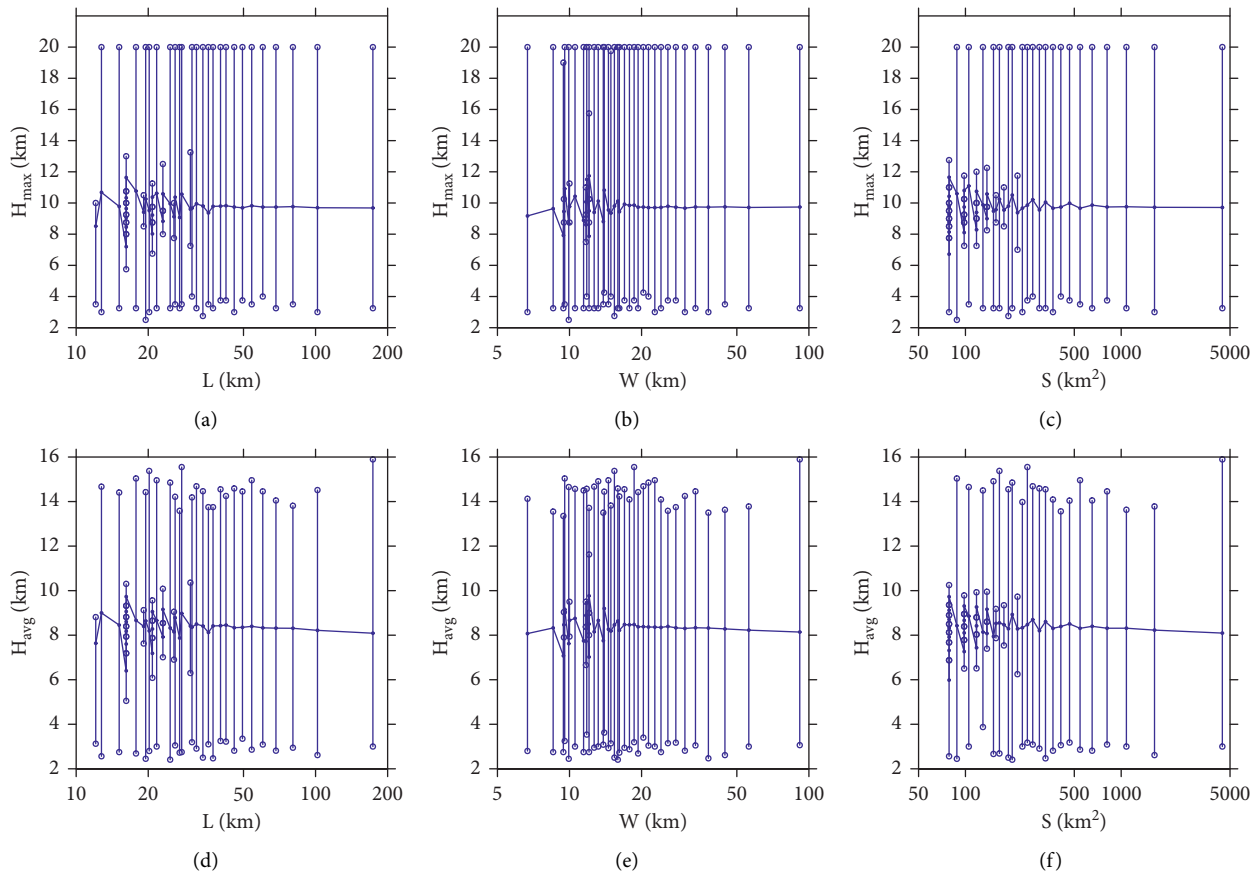

FIGURE 8: The relationship between H_{max} and L (a), H_{max} and W (b), H_{max} and S (c), H_{avg} and L (d), H_{avg} and W (e), and H_{avg} and S (f) on Tibetan Plateau from 1998 to 2015 based on the statistical principle of same samples in each interval at x axis.

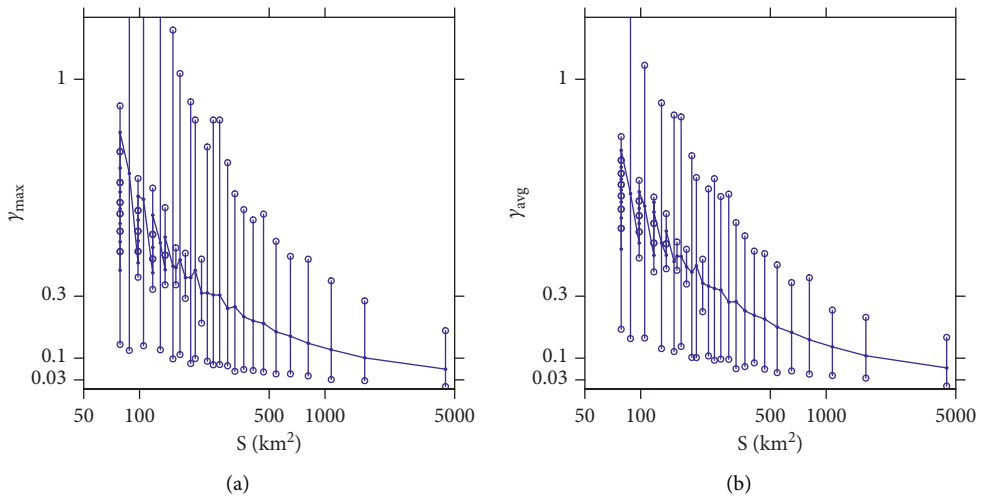

FIGURE 9: The relationship between γ_{max} and S (a) and γ_{avg} and S (b) on Tibetan Plateau from 1998 to 2015 based on the statistical principle of same samples in each interval at x axis.

less than 300 km^2, SPC tends to increase gradually, and then reaches about 80% steadily. Individually, the contribution of stratiform precipitation is also greater than convective precipitation. However, from the perspective of CAF and SAF, the contribution of convective precipitation is much greater than the area fraction of convective precipitation. It can be seen that the precipitation intensity of convective precipitation is still very large.

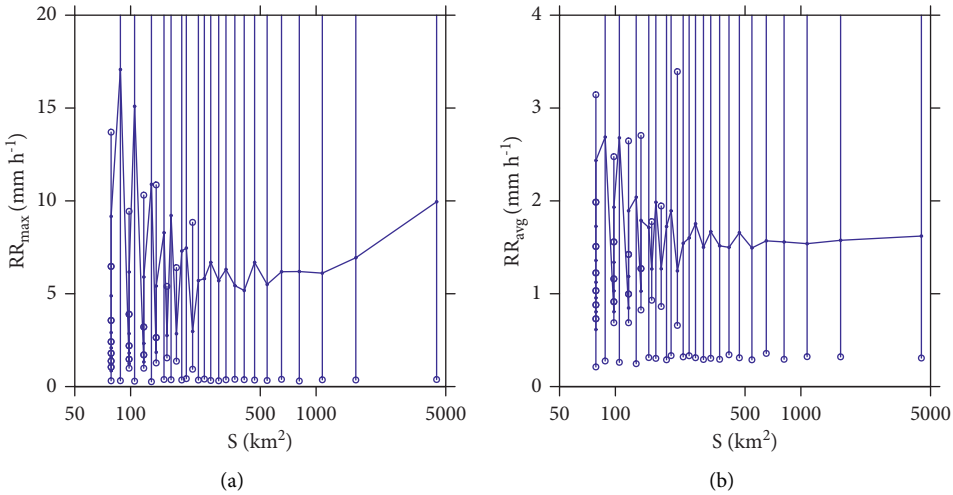

FIGURE 10: The relationship between RR_{max} and S (a) and RR_{avg} and S (b) on Tibetan Plateau from 1998 to 2015 based on the statistical principle of same samples in each interval at x axis.

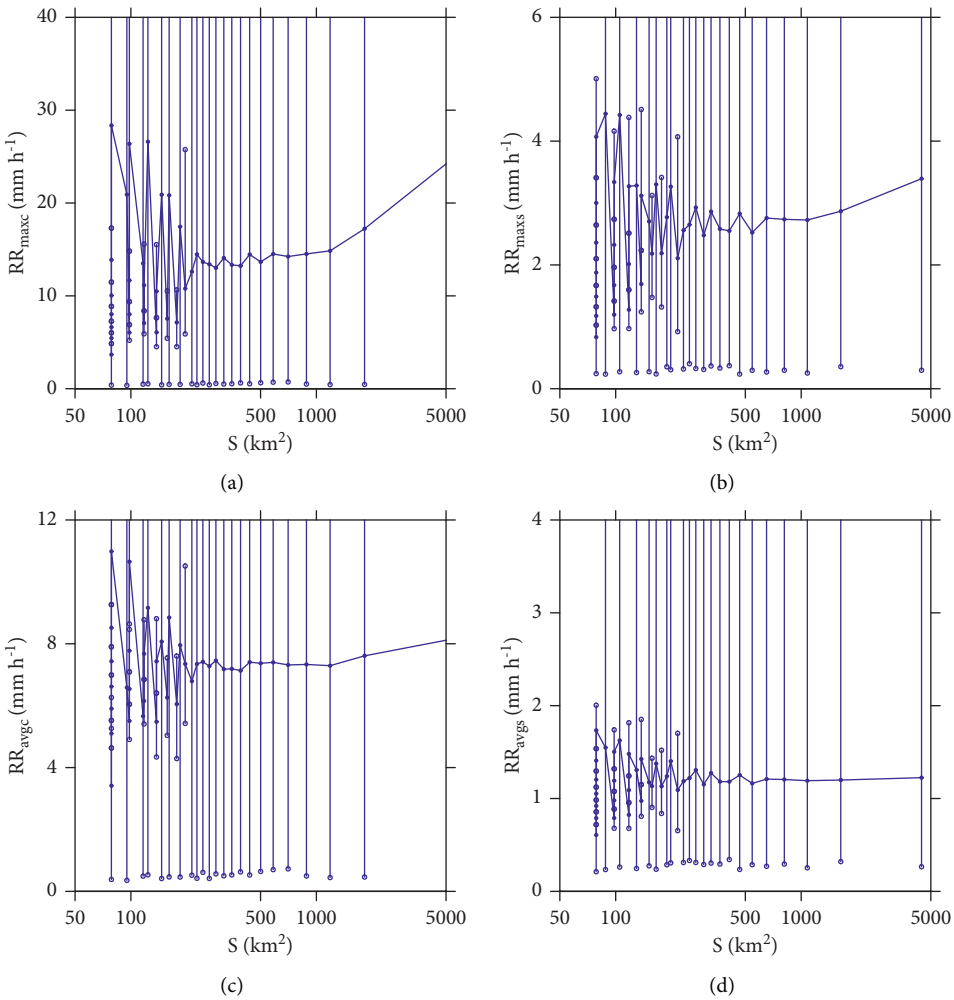

FIGURE 11: The relationship between RR_{maxc} and S (a), RR_{maxs} and S (b), RR_{avgc} and S (c), and RR_{avgs} and S (d) on Tibetan Plateau from 1998 to 2015 based on the statistical principle of same samples in each interval at x axis.

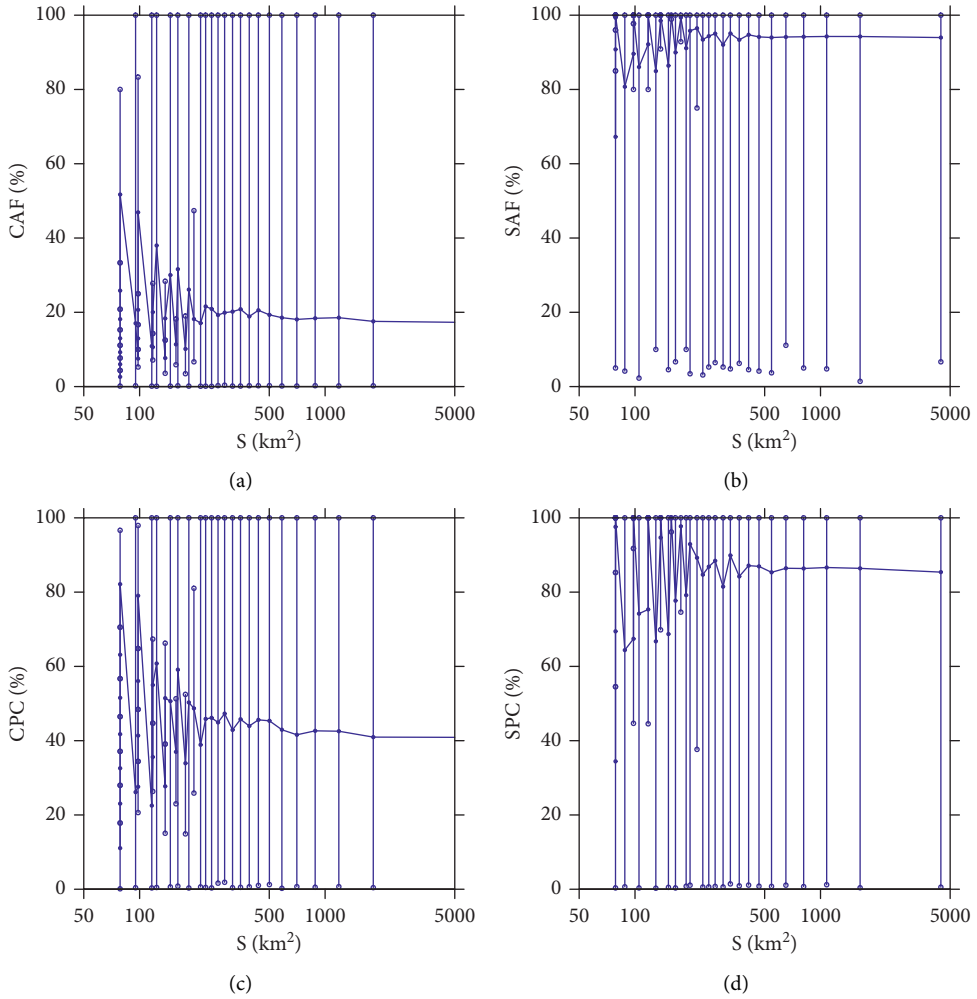

Figure 12: The relationship between CAF and S (a), SAF and S (b), CPC and S (c), and SPC and S (d) on Tibetan Plateau from 1998 to 2015 based on the statistical principle of same samples in each interval at x axis.

3.4. The Spatial Frequency Distribution of Rain Cells in Different Parameters. In order to understand the geometric and physical parameters of the above precipitation cloud, we further investigate the spatial frequency distribution of the precipitation cloud corresponding to the three different parameters. The first example is the spatial frequency distribution of precipitation clouds in different α, as shown in Figure 13. Based on the probability distribution function of α shown in Figure 3(c), three α ranges are selected, namely $\alpha \leq 0.4$, $0.4 < \alpha \leq 0.7$ and $\alpha > 0.7$. Figure 13(a) shows that precipitation clouds tend to be long ($\alpha \leq 0.4$) in the central and eastern plateau, and the frequency of such precipitation clouds is about 8%. The precipitation clouds on the southern slope of the plateau are mostly square ($\alpha > 0.7$), and the frequency of these precipitation clouds exceeds 56%, but the frequency of these precipitation clouds in the plateau is relatively low, only about 40% (Figure 13(c)). Precipitation clouds whose shapes tend to be between long strip and square shape ($0.4 < \alpha \leq 0.7$) are mainly distributed inside the plateau. The frequency of precipitation clouds is more than 54% (Figure 13(b)). By comparing the three situations shown in Figure 13, it is found that the long strip precipitation cloud accounts for the smallest proportion, followed by the square, and the precipitation cloud between the long strip and the square shape has the largest proportion. This is consistent with the result in Figure 3(c).

The second example is the spatial frequency distribution of precipitation clouds in different γ_{avg}. Based on the γ_{avg} probability distribution function shown in Figure 4(d), it is divided into three ranges: $\gamma_{\text{avg}} \leq 0.1$, $0.1 < \gamma_{\text{avg}} \leq 0.5$, and $\gamma_{\text{avg}} > 0.5$. Figure 14(a) shows that precipitation clouds in squatty appearance ($\gamma_{\text{avg}} \leq 0.1$)are mainly distributed in the marginal area of the eastern plateau, and the frequency of such precipitation clouds is about 16%. The precipitation clouds in lanky appearance ($\gamma_{\text{avg}} > 0.5$, Figure 14(c)) are concentrated in the southwestern part of the plateau, with a frequency of about 13%. Figure 14(b) shows that precipitation clouds that are neither squatty nor lanky appearance ($0.1 < \gamma_{\text{avg}} \leq 0.5$) mainly appear inside the plateau, with a frequency of more than 86%, which is consistent with the situation in Figure 4(d).

The third example is the spatial frequency distribution of precipitation clouds for different RR_{avg}, as shown in Figure 15. The results show that precipitation clouds with

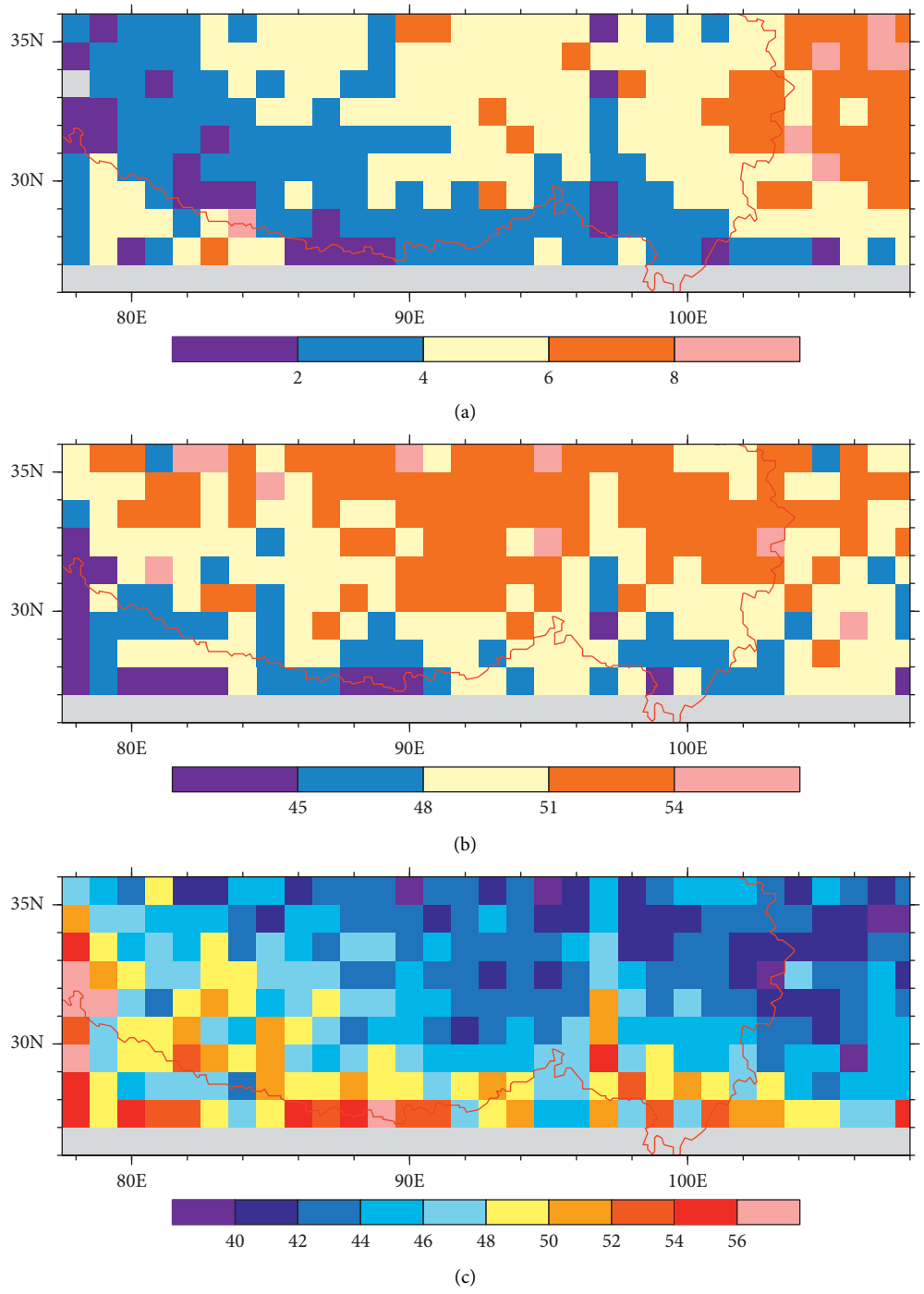

FIGURE 13: The spatial frequency distributions of precipitation clouds with (a) $\alpha \leq 0.4$, (b) $0.4 < \alpha \leq 0.7$, and (c) $\alpha > 0.7$. The red line represents the 3000-meter contour.

relatively small precipitation intensity ($RR_{avg} \leq 1.5\ mm{\cdot}h^{-1}$) dominate the plateau precipitation clouds, mainly distributed in the interior and east of the plateau, and the frequency of such precipitation clouds exceeds 60% (Figure 15(a)). Precipitation clouds with high precipitation intensity ($RR_{avg} > 4\ mm{\cdot}h^{-1}$) mainly appear in the southwest and eastern edges of the plateau, with a frequency of about 17% (Figure 15(c)). Precipitation clouds with moderate precipitation intensity ($1.5 < RR_{avg} \leq 4\ mm\ h^{-1}$) mainly appear on the southern slope of the plateau, with a frequency of more than 42% (Figure 15(b)). In summary, it is consistent with the result in Figure 5(b).

From the comprehensive analysis of Figures 13–15, precipitation clouds with moderate precipitation intensity mainly appear on the southern slope of the plateau and most of these precipitation clouds are square. Some precipitation clouds with lower precipitation intensity appear in the eastern plateau, and these precipitation clouds are mostly

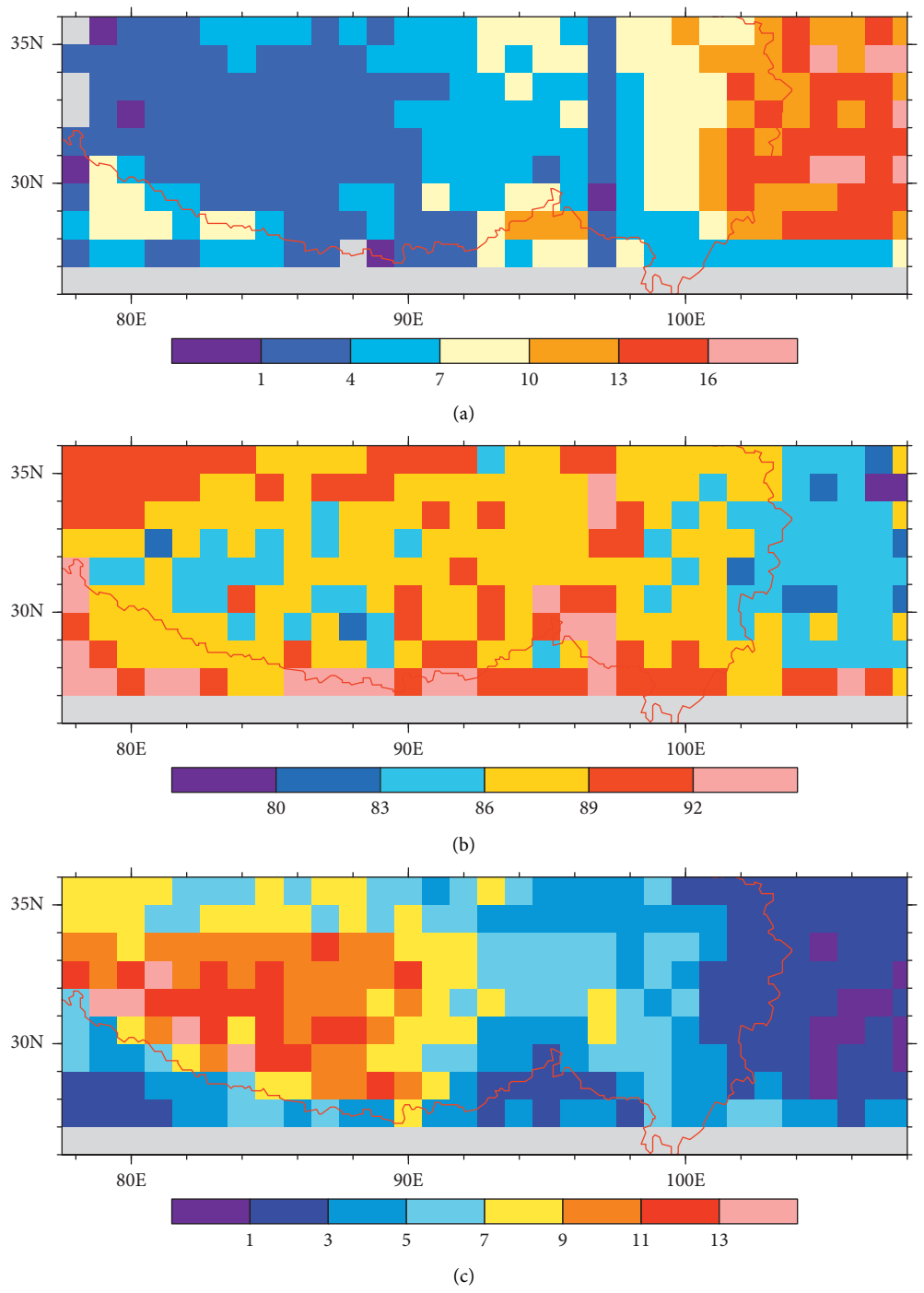

FIGURE 14: The spatial frequency distributions of precipitation clouds with (a) $\gamma_{avg} \leq 0.1$, (b) $0.1 < \gamma_{avg} \leq 0.5$, and (c) $\gamma_{avg} > 0.5$. The red line represents the 3000-meter contour.

having a long strip shape and its spatial shape tends to be squatty appearance; some appear in the interior of the plateau, and the horizontal shape of these precipitation clouds tends to be between square and long strip shape. Its spatial shape tends to be between the squatty appearance and lanky appearance. It can be seen that the geometric and physical parameters of precipitation clouds defined in this study are of great significance for revealing the spatial distribution characteristics and regional differences of precipitation clouds.

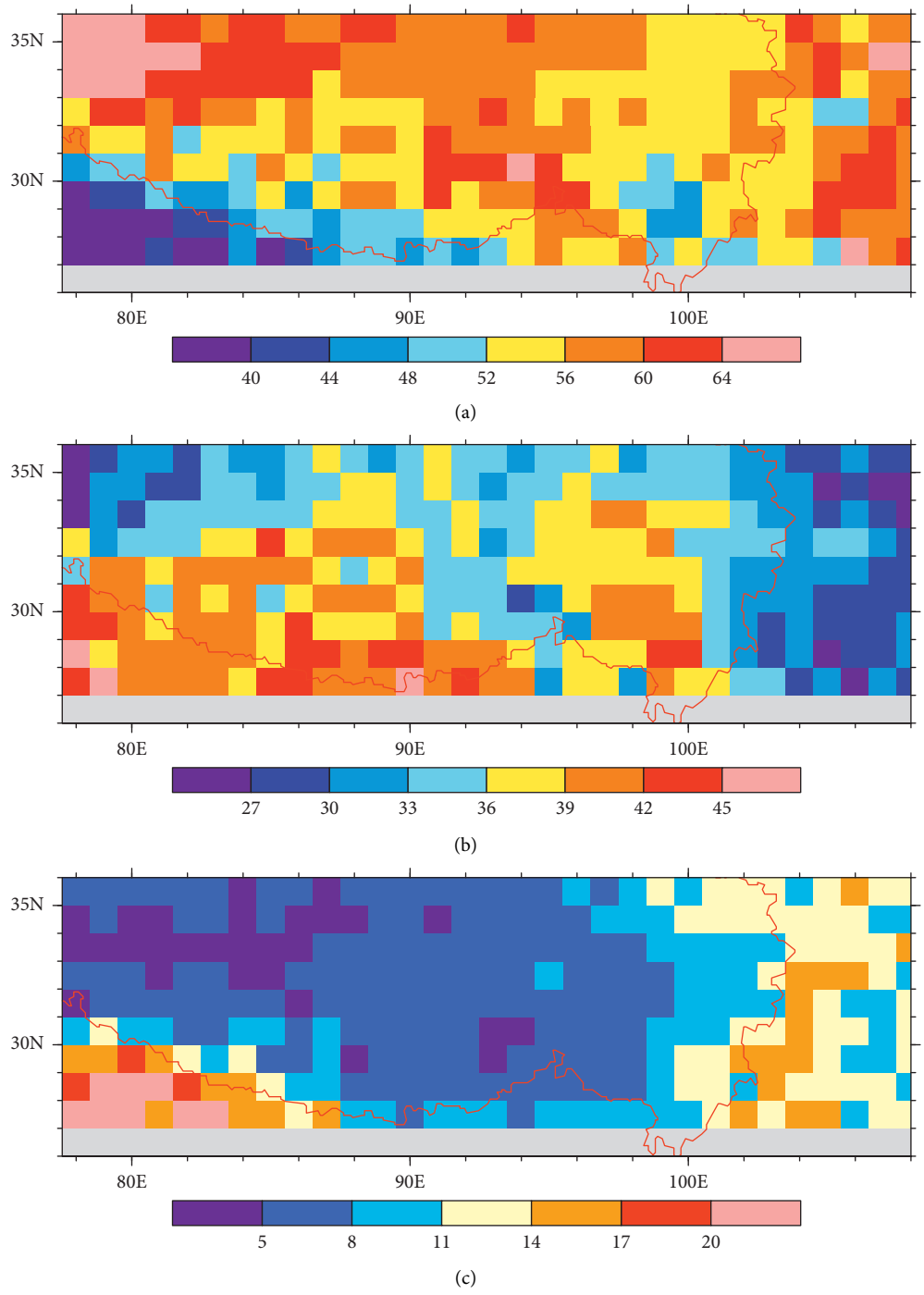

FIGURE 15: The spatial frequency distributions of precipitation clouds with (a) $RR_{avg} \leq 1.5$ mm h^{-1}, (b) $1.5 < RR_{avg} \leq 4$ mm h^{-1}, and (c) $RR_{avg} > 4$ mm h^{-1}. The red line represents the 3000-meter contour.

4. Conclusion

The precipitation system controlled by the weather system usually consists of precipitation clouds of various sizes. These precipitation clouds have complex shapes and different properties. It is important to understand the geometric and physical parameters of precipitation clouds, and the relationship between these parameters to have a deeper insight of the most basic characteristics of precipitation clouds. The studies of precipitation clouds are critical to the investigation of atmospheric circulation and latent heat. Meanwhile, the basic characteristics of precipitation clouds also provide observational basis for future weather forecasts. In this paper, the MBR method is used to identify precipitation clouds, and then the horizontal geometric parameters, vertical geometric parameters, and physical parameters are inverted to describe the basic characteristics of precipitation clouds.

The PDF of geometric parameters shows that about 60% of precipitation clouds appear on the dimension of 20 km in length and 15 km in width. The horizontal shapes of precipitation clouds tend to be between square shape and long strip shape. There are not many large precipitation clouds on the plateau. The average echo top height of precipitation clouds varies from 3 km to 13 km, and the peak appears at 9 km above the plateau. The clouds on the plateau are generally higher. The spatial morphology of precipitation clouds is mainly in lanky appearance.

The PDF of physical parameters shows that the probability of heavy rain on the plateau is much smaller than that of light rain. The difference between convective and stratiform precipitation is obvious. The probability distribution function of CAF decreases sharply as the CAF in the precipitation clouds increases, while the probability distribution function of SAF increases sharply as the SAF in the precipitation clouds increases. The contribution of convective precipitation in the same precipitation clouds is relatively low.

The relationship between geometric parameters shows that when L is greater than 25 km, there is a logarithmic linear relationship between the length L and the width W of the precipitation clouds. From the relationship between L, W, S, and α, we can conclude that the larger the horizontal scale of the precipitation clouds is, the closer its horizontal geometric shape is to quasisquare. As the horizontal scale increases, the horizontal structure of precipitation clouds becomes looser. The spatial morphology of precipitation clouds gradually changes from lanky appearance to squatty appearance as the area expands.

The relationship between physical parameters and geometric parameters shows that the average rainfall rate and maximum rainfall rate of precipitation clouds increase with the expansion of the area. When the raining area is larger than 500 km^2, the average rainfall rate remains at about 1.6 mm h^{-1}. The maximum and average rainfall rate of convective precipitation in the precipitation clouds increases with the expansion of the precipitation cloud area. For raining areas of the same size, the area fraction of convective precipitation and the contribution rate of the total precipitation are not as large as those of the stratiform precipitation.

The results also show that the precipitation clouds with moderate precipitation intensity mainly appear on the southern slope of the plateau and most of these precipitation clouds are square. Some precipitation clouds with lower precipitation intensity appear in the eastern plateau, and these precipitation clouds are mostly having a long strip shape and its spatial shape tends to be squatty appearance; some appear in the interior of the plateau, and the horizontal shape of these precipitation clouds tends to be between square and long strip shape. Its spatial shape tends to be between the squatty appearance and lanky appearance. In summary, the southern slope of the plateau is a large-value area where various types of precipitation clouds appear.

Data Availability

All figures were created using the NCAR Command Language (NCL) (2021) http://www.ncl.ucar.edu. The data can be obtained from the website https://pmm.nasa.gov/data-access/downloads/trmm for TRMM PR.

Conflicts of Interest

The authors declare that there are no conflicts of interest regarding the publication of this paper.

Acknowledgments

This work was financially supported by the Second Tibetan Plateau Scientific Expedition and Research (STEP) program (Grant no. 2019QZKK0103) and the National Natural Science Foundation of China Project (U20A2097, 42075087, and 41875108).

References

[1] R. T. Wetherald and S. Manabe, "Cloud feedback processes in a general circulation model," *Journal of the Atmospheric Sciences*, vol. 45, no. 8, pp. 1397–1416, 1988.

[2] E. Freud, F. D. Rosen, and M. O. Andreae, "Robust relations between CCN and the vertical evolution of cloud drop size distribution in deep convective clouds," *Atmospheric Chemistry and Physics*, vol. 8, no. 6, pp. 1661–1675, 2008.

[3] J. Chen, X. Wu, and Y. Yin, "Characteristics of heat sources and clouds over eastern China and the Tibetan plateau in boreal summer," *Journal of Climate*, vol. 28, pp. 7279–7296, 2015.

[4] Y. Li and M. Zhang, "Cumulus over the Tibetan plateau in the summer based on CloudSat-CALIPSO data," *Journal of Climate*, vol. 29, no. 3, pp. 1219–1230, 2016.

[5] D. L. Hartmann, M. E. Ockert-Bell, and M. L. Michelsen, "The effect of cloud type on Earth's energy balance: global analysis," *Journal of Climate*, vol. 5, pp. 1281–1304, 1992.

[6] T. Chen, W. B. Rossow, and Y. Zhang, "Radiative effects of cloud type variations," *Journal of Climate*, vol. 13, pp. 264–286, 2000.

[7] H. Sauvageot, F. Mesnard, and R. S. Tenório, "The relation between the area-average rain rate and the rain cell size distribution parameters," *Journal of the Atmospheric Sciences*, vol. 56, pp. 57–70, 1999.

[8] C. Capsoni, F. Fedi, and C. Magistroni, "Data and theory for a new model of the horizontal structure of rain cells for propagation applications," *Radio Science*, vol. 22, pp. 395–404, 1987.

[9] J. Awaka, "A three-dimensional rain cell model for the study of interference due to hydrometeor scattering," *J. Commun. Res. Lab.*vol. 36, pp. 13–44, 1989.

[10] H. L. Liu, W. Q. Zhu, and S. H. Yi, "Analysis on the climatic characteristics of clouds in China," *Acta Meteorologica Sinica*, vol. 61, no. 04, pp. 466–473+517-518, 2003.

[11] S. H. Wang, Z. G. Han, and Z. G. Yao, "Analysis of the macro characteristics of various clouds in China and surrounding areas based on CloudSat data," *Acta Meteorologica Sinica*, vol. 69, no. 05, pp. 883–899, 2011.

[12] H. K. Cai, X. Feng, and Q. L. Chen, "Spatial and temporal features of the frequency of cloud occurrence over China based on CALIOP," *Advances in Meteorology*, vol. 2017, Article ID 4548357, 11 pages, 2017.

[13] Y. H. Chen, Y. Chen, and J. P. Huang, "Cloud distribution and its changing trend in Northwest China," *Plateau Meteorology*, vol. 26, no. 4, pp. 741–748, 2007.

[14] P. Liu and Y. F. Fu, "Climatic characteristics of summer convective and stratiform precipitation in southern China based on measurements by TRMM precipitation radar," *Chinese Journal of Atmospheric Sciences*, vol. 34, no. 4, pp. 802–814, 2010.

[15] D. Z. Ye, "The thermal structure and the convective activity over Qinghai-Tibetan Plateau in summer and their interactions with large-scale circulation," *Chinese Journal of Atmospheric Sciences*, vol. 12, no. S1, pp. 1–12, 1988.

[16] Q. C. Long, Q. L. Chen, and K. Gui, "A case study of a heavy rain over the southeastern Tibetan plateau," *Atmosphere*, vol. 7, no. 9, 2016.

[17] Y. Sun, Q. L. Chen, and K. Gui, "Characteristics of water vapor in the UTLS over the Tibetan plateau based on AURA/MLS observations," *Advances in Meteorology*, vol. 2017, Article ID 3504254, 13 pages, 2017.

[18] Q. Chen, G. Gao, and Y. Li, "Main detrainment height of deep convection systems over the Tibetan plateau and its southern slope," *Advances in Atmospheric Sciences*, vol. 36, pp. 1078–1088, 2019.

[19] G. L. Gao, Q. L. Chen, and H. K. Cai, "Comprehensive characteristics of summer deep convection over Tibetan plateau and its south slope from the global precipitation measurement core observatory," *Atmosphere*, vol. 10, p. 9, 2019.

[20] H. X. Wu, *Low Clouds on the Qinghai-Tibet Plateau*, Meteorological Press, Beijing, China, 1985.

[21] X. Q. Zhang, L. L. Peng, and D. Zheng, "Temporal and spatial changes of total cloud amount on the Tibetan plateau and its influencing factors from 1971 to 2004," *Acta Geograghica Sinica (in Chinese)*, vol. 62, no. 9, pp. 959–969, 2007.

[22] L. Wei and Q. Zhong, "Climatological characteristics of clouds on the qinghai-tibet plateau," *Plateau Meteorology*, vol. 16, no. 1, pp. 11–16, 1997.

[23] W. B. Rossow and R. A. Schiffer, "ISCCP cloud data products," *Bulletin of the American Meteorological Society*, vol. 72, pp. 2–20, 1991.

[24] W. B. Rossow, A. W. Walker, and L. C. Garder, "Comparison of ISCCP and other cloud amounts," *Journal of Climate*, vol. 6, pp. 2394–2418, 1993.

[25] C. J. Hahn, W. B. Rossow, and S. G. Warren, "ISCCP cloud properties associated with standard cloud types identified in individual surface observations," *Journal of Climate*, vol. 14, pp. 11–27, 2001.

[26] R. X. Liu, Y. J. Liu, and B. Y. Du, "Analyze the cloud climate characteristics of the qinghai-tibet Plateau by ISCCP," *Journal of Nanjing Institute of Meteorology*, vol. 25, no. 2, pp. 226–234, 2002, in Chinese.

[27] Y. F. Yan, Y. M. Liu, and J. H. Lu, "Cloud vertical structure, precipitation, and cloud radiative effects over Tibetan Plateau and its neighboring regions," *Journal of Geophysical Research: Atmospheres*, vol. 121, pp. 5864–5877, 2016.

[28] Y. F. Fu, H. T. Li, and Y. Zi, "Case study of precipitation cloud structure viewed by TRMM satellite in a valley of the Tibetan Plateau," *Plateau Meteorology*, vol. 26, no. 1, pp. 98–106, 2007.

[29] X. Pan and Y. F. Fu, "Analysis on climatological characteristics of deep and shallow precipitation cloud in summer over the Tibetan Plateau," *Plateau Meteorology*, vol. 34, no. 5, pp. 1182–1189, 2015.

[30] Y. F. Fu, X. Pan, and G. S. Liu, "Characteristics of precipitation based on cloud brightness temperatures and storm tops in summer over the Tibetan Plateau," *Chinese Journal of Atmospheric Sciences*, vol. 40, no. 1, pp. 102–120, 2016.

[31] L. Feral, F. Mesnard, and H. Sauvageot, "Rain cells shape and orientation distribution in south-west of France," *Phys. Chem. Earth B: Hydrol. Oceans Atmos*, vol. 25, pp. 1073–1078, 2000.

[32] S. W. Nesbitt, R. Cifelli, and S. A. Rutledge, "Storm morphology and rainfall characteristics of TRMM precipitation features," *Monthly Weather Review*, vol. 134, pp. 2702–2721, 2006.

[33] C. T. Liu and E. Zipser, "Regional variation of morphology of organized convection in the tropics and subtropics," *Journal of Geophysical Research: Atmospheres*, vol. 118, pp. 453–466, 2013.

[34] Y. F. Fu, Y. L. Chen, and X. D. Zhang, "Fundamental characteristics of tropical rain cell structures as measured by TRMM PR," *J. Meteor. Res.*vol. 41, pp. 1–22, 2020.

[35] M. Hirose, S. Shimizu, and R. Oki, "Incidence-angle dependency of TRMM PR rain estimates," *Journal of Atmospheric and Oceanic Technology*, vol. 29, pp. 192–206, 2011.

[36] Y. F. Fu, X. Pan, and T. Xian, "Precipitation characteristics over the steep slope of the Himalayas in rainy season observed by TRMM PR and VIRS," *Climate Dynamics*, vol. 51, pp. 1971–1989, 2018.